Molecular Crystals and Liquid Crystals
Publication details, including instructions for authors and subscription information:
http://www.tandfonline.com/loi/gmcl16

Homogeneous Instability in Free Convection of Nematics—Effect of an Oblique Magnetic Field

U. D. Kini [a]
[a] Raman Research Institute, Bangalore, 560 080, India
Version of record first published: 20 Apr 2011.

To cite this article: U. D. Kini (1985): Homogeneous Instability in Free Convection of Nematics—Effect of an Oblique Magnetic Field, Molecular Crystals and Liquid Crystals, 128:1-2, 1-22

To link to this article: http://dx.doi.org/10.1080/00268948508082184

Mol. Cryst. Liq. Cryst., 1985, Vol. 128, pp. 1–22
0026-8941/85/1282–0001/$25.00/0

Printed in the United States of America

Homogeneous Instability in Free Convection of Nematics—Effect of an Oblique Magnetic Field

U. D. KINI

Raman Research Institute, Bangalore 560 080, India

(*Received October 26, 1984; in final form December 28, 1984*)

Using the continuum theory of uniaxial nematics, the homogeneous instability (*HI*) threshold of a flow aligning nematic (*FAN*), under free convection in a tilted sample whose boundaries are maintained at different temperatures, is studied as a function of strength and orientation of a magnetic field which is applied obliquely in a plane normal to the initial orientation of the nematic director. For a general field orientation, the *HI* threshold changes in magnitude when the sign of the temperature difference is reversed. Calculations are extended to a non-flow aligning nematic (*NFAN*) in which *HI* is possible under the action of a sufficiently strong destabilising field. The possibility of crossover between the field thresholds of two uncoupled modes is investigated as a function of the field orientation as well as the sign and magnitude of the temperature difference applied between the two plates. The case of nematics with negative diamagnetic anisotropy is briefly discussed.

1. INTRODUCTION

The homogeneous instability (*HI*) in nematic flow has been understood on the basis of the Ericksen-Leslie continuum theory of uniaxial nematics.[1–4] Since the discovery of *HI* in shear flow of a flow aligning nematic (*FAN*) by Pieranski and Guyon,[5] a number of experimental and theoretical studies have been reported in the literature[6–13] on different flows. (Refs. 4 and 13 are reviews on hydrodynamic instabilities in nematics.) These studies have established that *HI* and the related convective roll instability (*RI*) are caused by anisotropic viscous coupling between the director and velocity fields. A study by Horn *et al.*[14] has shown that *HI* can be produced by free convection which is set up in a thick tilted *FAN* sample whose boundaries are

maintained at different temperatures. A simple model which ignores secondary flow is found to account for the *HI* very well.[14]

Investigations by Pieranski and Guyon and by Guyon *et al.*[15-17] have shown that *HI* is not ordinarily possible in a non-flow aligning nematic (*NFAN*) due to the break down of the positive feed-back mechanism caused by the stabilising action of shear on the initial director orientation against homogeneous perturbation; *RI* can of course occur at sufficiently elevated shear rates. However, the continuum theory does not rule out the possibility of *HI* in shear flow and in plane Poiseuille flow of a *NFAN* in the presence of a sufficiently strong destabilising magnetic field which is applied along the flow or normal to the plates.[18] A calculation of the *HI* threshold in free convection shows[19] that *HI* is possible in a *NFAN* under the action of a destabilising field and that at sufficiently high stabilising shear rate and destabilising field a generally unfavourable instability mode may be observed.

Recently, the *oblique field configuration* considered by Deuling *et al.*[20] in the static Freedericsz transition has been theoretically studied in connection with *HI* in shear flow of nematics.[20] It turns out that for a general orientation of the oblique field, the magnitude of the *HI* threshold changes when the sign of shear rate is reversed. In particular, in the case of a *NFAN* the crossover between the field thresholds of two uncoupled instability modes may depend strongly on the field orientation.

In this communication, the linearised differential equations governing homogeneous perturbations are solved numerically for the case of free convection in the presence of an oblique magnetic field which is applied in a plane normal to the initial director orientation. For a *FAN* the *HI* shear threshold (which is proportional to the temperature difference ΔT between the plates) is studied as a function of field strength and orientation. In the case of a *NFAN* the *HI* field thresholds of both the uncoupled modes are studied as functions of the applied shear rate and field orientation. Due to non-availability of complete viscoelastic data for nematics with negative diamagnetic susceptibility anisotropy, this case is briefly discussed.

2. DIFFERENTIAL EQUATIONS, BOUNDARY CONDITIONS AND SOLUTION

The nematic with initial director orientation $\mathbf{n}_0 = (1, 0, 0)$ is confined between plates $z = \pm h$ which are maintained at temperatures T_2 and T_1 respectively; $\Delta T = T_1 - T_2$; $T(z)$ is the temperature field in

the sample. The plates are tilted so that they make an angle φ with the vertical. The uncompensated y component of the buoyancy force causes free convection to set in even for small ΔT, if the sample is sufficiently thick. Adopting the Boussinesque approximation the temperature variation of all material parameters except that of density is ignored. For sufficiently small ΔT, far away from the sample edges and in the absence of perturbations, the velocity field due to free convection as also the temperature field are represented by

$$\begin{aligned} \mathbf{v}_0 &= [0, v_{y0}(z), 0], \\ v_{y0}(z) &= \overline{G}(z^3 - zh^2), \\ S(z) &= \overline{G}(3z^2 - h^2), \\ T(z) &= -(\Delta T)z/2h + (T_1 + T_2)/2 \\ \overline{G} &= \rho g \beta (\Delta T)(\cos\varphi)/12\eta_2 h \end{aligned} \tag{1}$$

where ρ is the density, g the acceleration due to gravity, β the thermal expansion coefficient and $\eta_2 = \alpha_4/2$ a Miesowicz viscosity coefficient of the nematic; $S(z) = v_{y0,z}$, the shear rate at a point z in the fluid, is directly proportional to ΔT. The z component of the buoyancy force is balanced by the pressure gradient along z. In the presence of homogeneous perturbations the director and velocity fields become $\mathbf{n} = (1, n_y, n_z)$, $\mathbf{v} = (v_x', v_{y0}, 0)$ where n_y, n_z and v_x' are small and are functions of z alone. Time dependence of perturbations is ignored keeping in view the non-oscillatory nature of the instability. It is possible, in principle, to consider fluctuations in v_{y0} and T. As shown earlier[19] these perturbations can be ignored without loss of generality in all cases of practical interest. With an oblique magnetic field $\mathbf{H}(\psi) = (0, H_\perp \cos\psi, H_\perp \sin\psi)$ acting in the yz plane, the torque and force equations become[21]

$$h^2\Gamma_y/K_1 = -d^2n_z/d\xi^2 - A_1 n_z - n_y[A_2 + A_3(3\xi^2 - 1)] + A_7 b = 0 \tag{2}$$

$$h^2\Gamma_z/K_2 = d^2n_y/d\xi^2 + A_4 n_y + n_z[A_5 + A_6(3\xi^2 - 1)] = 0 \tag{3}$$

$$dv_x'/d\xi + A_8(3\xi^2 - 1)n_y h/\eta_1 = bh/\eta_1 \tag{4}$$

$$S_\psi = \sin\psi,\ C_\psi = \cos\psi,$$

$$A_1 = \chi_a h^2 H_\perp^2 S_\psi^2/K_1,$$

$$A_2 = \chi_a h^2 H_\perp^2 S_\psi C_\psi/K_1$$

$$A_3 = -\alpha_3 h^3 \rho g \beta(\Delta T)(\cos\varphi)/12\eta_1 K_1,$$

$$A_4 = \chi_a h^2 H_\perp^2 C_\psi^2/K_2$$

$$A_5 = \chi_a h^2 H_\perp^2 S_\psi C_\psi/K_2,$$

$$A_6 = -\alpha_2 h^3 \rho g \beta(\Delta T)\ (\cos\varphi)/12\eta_2 K_2,$$

$$A_7 = \alpha_3 h^2/\eta_1 K_1,$$

$$A_8 = (\eta_1 - \eta_2) h \rho g \beta(\Delta T)\ (\cos\varphi)/12\eta_2 \qquad (5)$$

where Γ is the total torque exerted on the nematic director, $\xi = z/h$, K_1, K_2 the splay and twist elastic constants, α_2, α_3, $\eta_1 = (\alpha_3 + \alpha_4 + \alpha_6)/2$ viscosity coefficients, χ_a the diamagnetic susceptibility anisotropy and b = (an indeterminate) constant equal to the viscous stress σ'_{zx} acting in the plane (zx) normal to the shear plane.

Throughout this communication ψ is measured in radian. All quantities are measured in cgs units. In particular, elastic constants K_1 and K_2 are measured in dyne, (ΔT) in degree centigrade, viscosities α_2, α_3, η_1, η_2 in poise; magnetic field $H_\perp$ is measured in gauss.

Assuming firm anchoring of the director and no slip at the boundaries, the following conditions are imposed on the perturbations:

$$n_y(\pm 1) = n_z(\pm 1) = v'_x(\pm 1) = 0 \qquad (6)$$

The differential equations (2)–(4) are analogous to the equations which govern perturbations in shear flow.[21] This is because, in both cases the primary velocity v_{y0} is an odd function of z and the primary shear rate $v_{y0,z}$ an even function. Hence most conclusions here automatically follow those of ref. 21, qualitatively. Eqs. (2)–(4) show that if $\psi = 0$ or $\pi/2$, at a given field $H_\perp$, the magnitude of the shear threshold (threshold value of ΔT) for a *FAN* will remain unaltered when the direction of flow is reversed in the sample (i.e. when the sign of ΔT is reversed, i.e. when the temperatures of the two plates

are interchanged). This is of course trivially valid for the field-free case. A similar conclusion holds for the field threshold for a *NFAN*; at $\psi = 0$ or $\pi/2$, the magnitude of the field threshold (threshold value of $H_\perp$) does not change when the sign of ΔT is reversed.

However, for a general value of ψ (not 0, $\pi/2$ or π) there is no transformation which can take Eqs. (2)–(4) into themselves when the sign of the shear rate is reversed. This indicates that in the case of a *FAN*, at a given value of $H_\perp$, when the sign of shear rate is reversed, the magnitude of the shear threshold will change. A similar statement can be made for a *NFAN*; for a given magnitude of the shear rate and at a general field orientation ψ, the magnitude of the field threshold will change when the sign of the shear rate is reversed. The only transformation which leaves the equations invariant is the trivial one, $\psi \rightarrow \psi + \pi$, showing that it is sufficient to restrict ψ to the range $0 \leqslant \psi \leqslant \pi$. As in the case of shear flow,[21] Eqs. (2)–(4) can support two uncoupled modes:

$$\text{Mode 1: } n_y, n_z \text{ even; } v_x' \text{ odd; } b \neq 0$$

$$\text{Mode 2: } n_y, n_z \text{ odd; } v_x' \text{ even; } b = 0$$

It is possible to solve the differential equations for shear flow[21] by series method and by the calculation of wave vectors mainly because the shear rate is constant in the sample. This presents a set of differential equations with constant coefficients which can be homogenised by a simple transformation, even for Mode 1 (see Appendix I, ref. 21). In the present case only Mode 2 is governed by a set of homogeneous differential equations; the differential equations governing Mode 1 cannot be easily homogenised, as the equations have variable coefficients owing to the shear rate being quadratic in the independent variable. This rules out series solution method for Mode 1, though Mode 2 can still be solved by this method. In either case, it is not possible to calculate the wave vectors of perturbations at threshold (by seeking solutions $\sim \exp iq\xi$).

The orthogonal collocation method (see for instance, Finlayson[22] and Tseng *et al.*[23]) is therefore used, with the zeroes of the Legendre polynomial P_{24} as collocation points. This allows conversion of the differential equations into a set of $2N$ linear equations ($N = 24$) whose solution by standard numerical techniques leads to a computation of the threshold. All computations have been performed with double precision arithmetic on the DEC-1090 computer at the Indian Institute of Science, Bangalore. For Mode 1, n_y and n_z (scaled by b)

are calculated from Eqs. (2), (3) and (6). Using Eqs. (4) and (6) the threshold condition is realised by iteration. For Mode 2, Eqs. (2), (3) and (6) result in a $2N \times 2N$ matrix the vanishing of whose determinant yields the threshold. For either mode, normalised profiles of perturbations at threshold (*NP*) can be calculated. This has been done retaining the relative signs of the different profiles.

Keeping in mind the results of ref. 20, the effect of the magnetic field is measured by the square of the dimensionless magnetic wave vector

$$R_m = A_1 + A_4 = \chi_a h^2 H_\perp^2 (K_1 C_\psi^2 + K_2 S_\psi^2)/K_1 K_2 \qquad (7)$$

For a nematic with $\chi_a > 0$, R_m takes the value $\pi^2/4$ at the static Freedericsz transition. The effect of shear rate is measured by the dimensionless number

$$G = (A_3 A_6)^{1/2} = h^3 \rho g \beta (\Delta T) (\cos \varphi) (\alpha_2 \alpha_3 / \eta_1 \eta_2 K_1 K_2)^{1/2}/12 \qquad (8)$$

for a *FAN*. In the case of a *NFAN*,

$$G = (-A_3 A_6)^{1/2} \qquad (9)$$

is used for measuring the effect of shear rate. This definition of G differs quantitatively from that of ref. 19. The present definition follows the definition of the Ericksen number for shear flow in refs. 9 and 21. Clearly, G is the nematic counterpart of the Grasshof number defined for isotropic liquids.[24]

3. RESULTS FOR A *FAN* (MBBA)

MBBA has been chosen as the model nematic representing this class. The material constants are assumed to have the following values (see refs. 9 and 14 for relevant literature): $K_1 = 6 \times 10^{-7}$, $K_2 = 3 \times 10^{-7}$, $\chi_a = 1.15 \times 10^{-7}$, $\alpha_2 = -0.775$, $\alpha_3 = -0.012$, $\eta_1 = 0.248$, $\eta_2 = 0.416$; $\rho = 1.088\ \text{gm cm}^{-3}$, $\beta = 9 \times 10^{-4}\ \text{degree}^{-1}$. The sample thickness $2h$ and g are assumed to have the values 0.1 cm and 980 cm sec^{-2} respectively, throughout this work. As Mode 2 has a higher threshold than Mode 1 for all field strength and orientation, only Mode 1 will be considered for MBBA. For given $H_\perp$ and ψ, the shear rate (or equivalently ΔT) is varied until the condition of compatibility of Eqs. (2)–(6) is satisfied. This gives the *HI* threshold $(\Delta T)_c$ or

equivalently the critical value G_c of the dimensionless number G. For MBBA, in the field-free case, $(\Delta T)_c \cos \varphi \approx 0.61°C$ or $G_c \approx 4.35$ in fair agreement with ref. 14. (For MBBA parameters, $(\Delta T) \cos \varphi = 1°C$ is equivalent to $G \approx 7$.)

It must be mentioned that it is possible to solve for Mode 1 by putting $b = 0$. In this case, the solution proceeds on the lines of that of Mode 2. From Eqs. (2), (3) and (6) one gets $|(\Delta T)_c| \cos \varphi \approx 0.52°C$ or $|G_c| \approx 3.81$ (ref. 19). Through this is in excellent agreement with the experimental result of ref. 14, it cannot be regarded as the Mode 1 threshold because the solution to the problem is not complete; with $b = 0$, the n_y and n_z profiles can be calculated but the v_x' profile cannot be calculated from Eq. (4). As the threshold is known from Eqs. (2)–(3), Eq. (6) imposes a restriction on material parameters and sample thickness. Also, as v_x' is an integral part of the picture, it must not be ignored. Taking $v_x' = 0$ *ab initio* is also not very realistic. Thus, for solving for the Mode 1 threshold b is assumed to be non-zero. This does lead to an elevated threshold but facilitates a complete solution of the problem through a full determination of all *NP*s. Finally, it must be pointed out that b is an indeterminate constant which arises out of an integration of the x component of the force equation and cannot, therefore, be equated to zero. Symmetry dictates the absence of b from the Mode 2 picture but allows its presence with Mode 1. With $b \neq 0$ when $|G|$ is increased from zero, the threshold condition shows a singularity at $|G| \approx 3.81$ for the field-free case. On further increasing $|G|$, the first zero of the compatibility equation is found at $|G_c| \approx 4.35$ and this is chosen as the Mode 1 threshold. (There is a striking similarity with shear flow; Appendix I, ref. 21. The threshold condition for shear flow involves the *tan* function and this makes the reason for the occurrence of the singularity rather obvious. In the present case it is not easy to make out the reason for the occurrence of the singularity.)

Figure 1 shows the variation of G_c with the field orientation ψ at $H_\perp = 50$ gauss. This field has been chosen as it is close to the twist Freedericsz transition. G_c shows a marked variation with ψ. The threshold has extrema near $\psi = 0.8$ and 2.4 ($\approx \pi/4$ and $3\pi/4$, respectively). At general ψ, there is a noticeable difference in the magnitude of G_c for positive and negative G, especially near the two extrema. It must be remembered that though $H_\perp$ is constant, R_m varies with ψ (Eq. 7).

Figure 2 illustrates the dependence of G_c on R_m (or equivalently on $H_\perp$) at different orientations ψ. For $G > 0$, at $\psi = 0, \pi/2, 2.9$, G_c decreases from its field-free value of 4.35 as R_m increases from

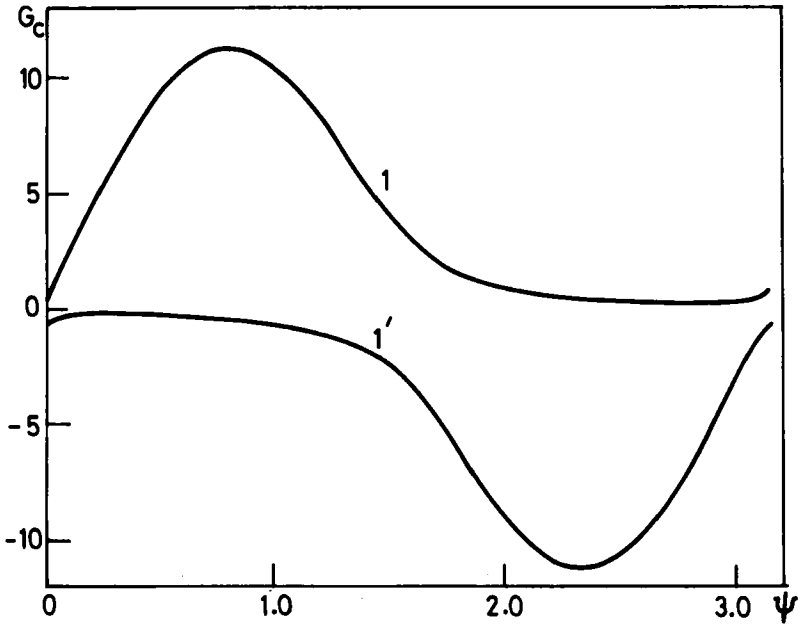

FIGURE 1 Plot of Mode 1 *HI* shear threshold G_c as a function of field orientation ψ for a *FAN* (MBBA) at field strength $H_\perp = 50$ gauss.

zero. When $R_m \to \pi^2/4$ which is the corresponding Freedericsz threshold, $G_c \to 0$. But at $\chi = 0.8$ and 1.4, G_c *increases* continuously with R_m and shows no tendency to decrease even when $R_m \to \pi^2/4$. The variation of $|G_c|$ for $G < 0$ is similar except that $|G_c|$ decreases to zero with increasing R_m at $\psi = 0, 0.3, \pi/2$, but increases at $\psi = 1.75$ and 2.2. The present calculation reflects a thought experiment in which the magnetic field $H_\perp$ is applied first and then the temperature difference $|\Delta T|$ increased from zero till the HI threshold $|G_c|$ is attained. Hence, values of $R_m > \pi^2/4$ are not of physical significance. Thus all curves in Figure 2 have been truncated at $R_m = \pi^2/4$, which corresponds to the static Freedericsz limit for the given field orientation.

The case of free convection is complicated by the fact that shear rate can be positive, zero or negative depending upon the point under study in the sample. However, the *HI* mechanism is found to work in the same way at all points. Hence, a tentative discussion is confined to the case $(\Delta T) \cos \varphi > 0$ and to a point situated close to the sample centre where $3\xi^2 - 1 < 0$. As the *HI* mechanism is well known[5-17] the discussion is brief. Let $0 < \psi < \pi/2$. A fluctuation $n_z > 0$ creates

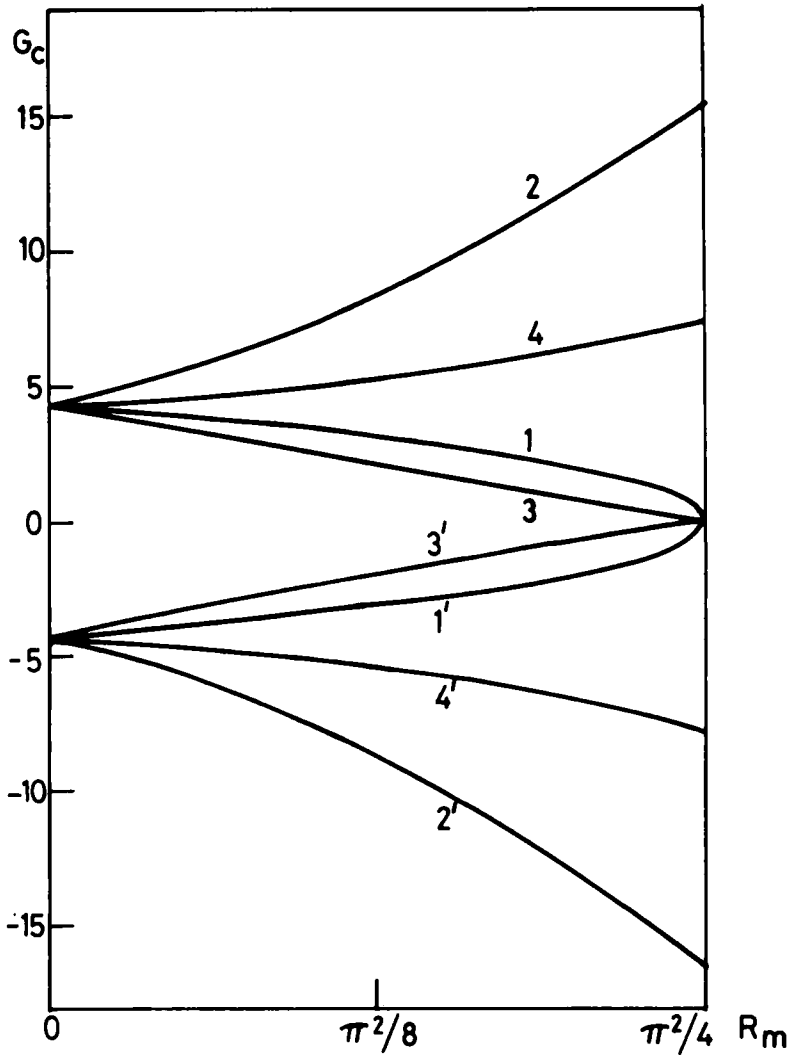

FIGURE 2 Plot of Mode 1 *HI* shear threshold G_c vs R_m, the dimensionless magnetic wave vector for different field orientations ψ. *FAN*.MBBA.
$G_c > 0 \cdot \psi$ = (1)0, $\pi/2$(2) 0.8(3) 2.9(4) 1.4
$G_c < 0 \cdot \psi$ = (1′)0, $\pi/2$(2′) 2.2(3′) 0.3(4′) 1.75

a torque $\Gamma_z^{(1)} \sim n_z[A_5 + A_6(3\xi^2 - 1)]$ (Eq. 3). As $\alpha_2 < 0$ and $|\alpha_2| \sim 1$, the viscous term containing A_6 can outbalance the magnetic term A_5 so that $\Gamma_z^{(1)} < 0$ and gives rise to $n_y < 0$. This in turn creates a torque $\Gamma_y^{(1)} \sim -n_y[A_2 + A_3(3\xi^2 - 1)]$ (Eq. 2). When ψ is close to 0 or $\pi/2$, the magnetic term A_2 is small and the sign of the torque $\Gamma_y^{(1)}$ will be determined by the viscous term. As $\alpha_3 < 0$, $\Gamma_y^{(1)} < 0$ showing that this torque will further enhance the original n_z fluctuation and thus complete the positive feed-back mechanism. Suppose on the other hand $\psi \approx \pi/4$ and $H_\perp$ is close to the Freedericksz limit. The magnetic term is no longer small. As $A_3 \propto \alpha_3$ and $|\alpha_3| \ll 1$, the magnetic term may outweigh the viscous term. In this case, $\Gamma_y^{(1)} > 0$ and the positive feed-back mechanism is no longer positive. This may tentatively explain the anomalous stabilising effect of $H_\perp$ when ψ is close to $\pi/4$. The discussion for $G < 0$ and for other regions of the sample (where $3\xi^2 - 1 > 0$) follows similarly.

Figure 3 contains the *NP*s for Mode 1 at different field strengths and orientations. At suitable values of field and orientation, *NP*s for $G < 0$ are similar. As both G_c and R_m are small the profiles do not show much change when field strength and orientation are varied. Only the profile of n_z at $\psi = 0.8$ shows strong distortion. By comparison with shear flow,[21] one might say that the distortion is the result of increasing 'wave vector.' However, this cannot be asserted here as the wave vectors of deformation cannot be calculated.

Before going over to the case of a *NFAN*, mention may be made of the prediction of the present linearised model for a *FAN* having $\chi_a < 0$. So far, studies on such nematics have dealt with dielectric and diamagnetic susceptibilities, elastic constants and magnetic resonance (see for instance refs. 25–27; for studies on lyotropic systems see for example, ref. 28 and references therein). However, data on viscosity coefficients of nematics with $\chi_a < 0$ do not seem to be available. In the present work a model calculation has been performed with MBBA parameters with the sign of χ_a reversed. The results are similar to those of ref. 21 and can be briefly summarised as follows: A field $H_\parallel$ applied along x has a destabilising influence. The effect of $H_\parallel$ is included by equating $H_\perp$ to zero and adding terms $\chi_a H_\parallel^2 h^2 n_z / K_1$ and $-\chi_a H_\parallel^2 h^2 n_y / K_2$ to Eqs. (2) and (3) respectively. The field $H_\parallel$, like the field $H_\perp$ for general ψ, couples to both the director fluctuations. But the coupling is not exactly similar; the field $H_\parallel$ does not enter cross terms such as A_2 and A_5. On increasing $H_\parallel$, G_c decreases and tends to zero when $H_\parallel$ approaches the twist Freedericsz threshold ($\approx$51 gauss). The decrease to zero does not occur at the splay threshold because $K_2 < K_1$ for MBBA parameters. Under the action of a

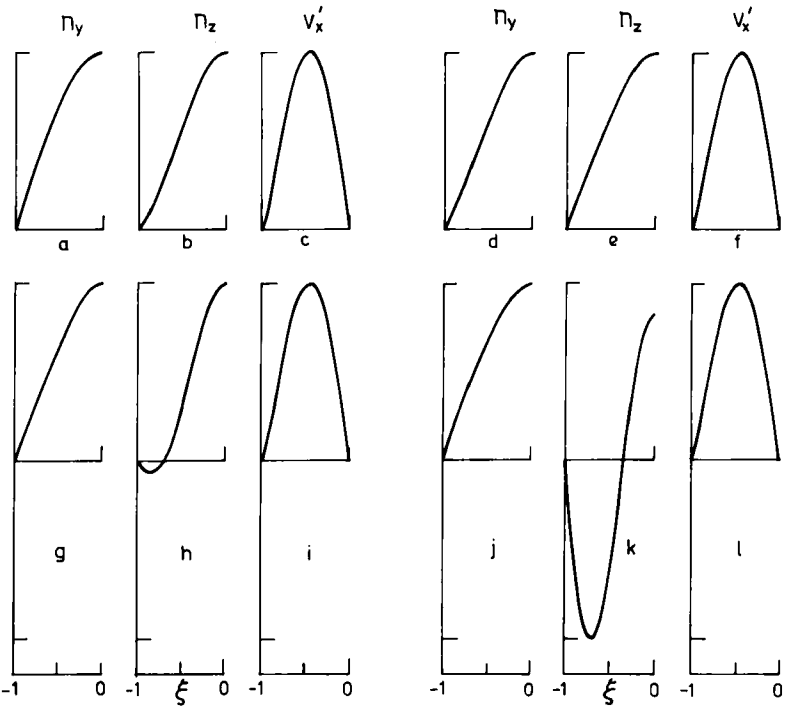

FIGURE 3 *FAN*.MBBA. Normalised profiles of Mode 1 perturbations at shear threshold for different fields $H_\perp$ and orientations $\psi \cdot X_c = (\Delta T)_c \cos \varphi$.
(a), (b), (c) $H_\perp = 50$, $\psi = 0$, $X_c = 0.107$; $G_c = 0.755$, $R_m = 2.4$; the same profiles suffice for $\psi = 2.9$, $X_c = 0.031$, $G_c = 0.22$, $R_m = 2.33$ except that $-n_z$ is given by the dotted line in (b).
(d), (e), (f) $H_\perp = 50$, $\psi = \pi/2$, $X_c = 0.45$, $G_c = 3.17$, $R_m = 1.12$.
(g), (h), (i) $H_\perp = 70$, $\psi = 1.4$, $X_c = 1.03$, $G_c = 7.3$, $R_m = 2.42$
(j), (k), (l) $H_\perp = 50$, $\psi = 0.8$, $X_c = 1.58$, $G_c = 11.2$, $R_m = 1.8$

field $H_\perp$ the present case is physically different from that of a *FAN* with $\chi_a > 0$. When the sign of χ_a is reversed there is no transformation which can take Eqs. (2) and (3) into themselves. As $R_m < 0$, there is also no Freedericsz threshold (Eq. 7). The results are stated for $G > 0$; results for negative shear rates are similar. At low fields $H_\perp$, Mode 1 is always favourable. When $\pi/2 < \psi < \pi$, G_c increases with R_m and at sufficiently high field strength, Mode 2 threshold becomes lower than that of Mode 1. A crossover from Mode 1 to Mode 2 thus seems possible. But when $0 < \psi < \pi/2$, Mode 1 is always favourable. Also, in this ψ range, when R_m increases, G_c decreases tending to a lower limiting value when R_m becomes large. Thus the behaviour of a *FAN* with $\chi_a < 0$ is likely to be strikingly different from that of a

FAN with $\chi_a > 0$, in the presence of an oblique field. The crossover from Mode 1 to Mode 2 can be qualitatively understood by writing the *HI* shear threshold as $S_c \sim Kq^2/\eta h^2$ where q is the dimensionless wave vector; K and η are average elastic and viscosity coefficients respectively. Using Eq. (8) and dimensional analysis, the shear threshold can be written as $G_c \sim q^2$. Thus, roughly speaking, the larger the wave vector of distortion the higher the threshold. An examination of the *NP*s shows that crossover from Mode 1 to Mode 2 is accompanied by greater distortion of the Mode 1 profiles as compared to the Mode 2 profiles. This crossover is reminiscent of a similar crossover between two uncoupled modes predicted by Leslie[29] for *HI* in a different flow situation.

4. RESULTS FOR A *NFAN* (HBAB)

HBAB has been chosen to represent this class of nematics. The material constants have been chosen to have the following values: $K_1 = 8.44 \times 10^{-7}$, $K_2 = 4.78 \times 10^{-7}$, $\chi_a = 0.745 \times 10^{-7}$ cgs, $\alpha_2 = -0.327$, $\alpha_3 = 0.0034$, $\eta_1 = 0.0881$, $\eta_2 = 0.1373$ (see ref. 30 for relevant literature); for the remaining two parameters, the values assumed are $\rho = 1.0$ gm cm^{-3} and $\beta = 10^{-3}$ degree^{-1}, as the experimental values are not known. As has been clearly shown,[15-17] *HI* is not ordinarily possible in a *NFAN* as the positive feed-back mechanism fails due to stabilising action of the imposed shear rate on the initial director orientation against homogeneous perturbations. However, taking a cue from earlier work[18,19,20] the effect of a destabilising field $H_\perp$ is investigated and as expected, for a given G (Eq. 9) the *HI* threshold is attained when R_m exceeds a critical value R_{mc}. The possibility of crossover between modes makes calculation for both the uncoupled modes imperative.

Figure 4 illustrates the variation of R_{mc} with field orientation ψ at $|G| = 0.49$ and 2.45 ($|(\Delta T) \cos \varphi| = 0.1$°C and 0.5°C respectively). As is clear, for HBAB parameters, $\Delta T = 1.0$°C is equivalent to $G = 4.9$. At the lower shear rate, Mode 1 threshold is less than the Mode 2 threshold for all field orientations. The thresholds of both the modes show the same qualitative variation with ψ, but the Mode 2 threshold varies very little. At the higher shear rate, depending upon the sign of G and the ψ range, Mode 2 is found to be more favourable than Mode 1. There is also a more marked variation in the Mode 2 threshold, but not as much as in the Mode 1 threshold which increases very steeply at some values of ψ. The curves for G

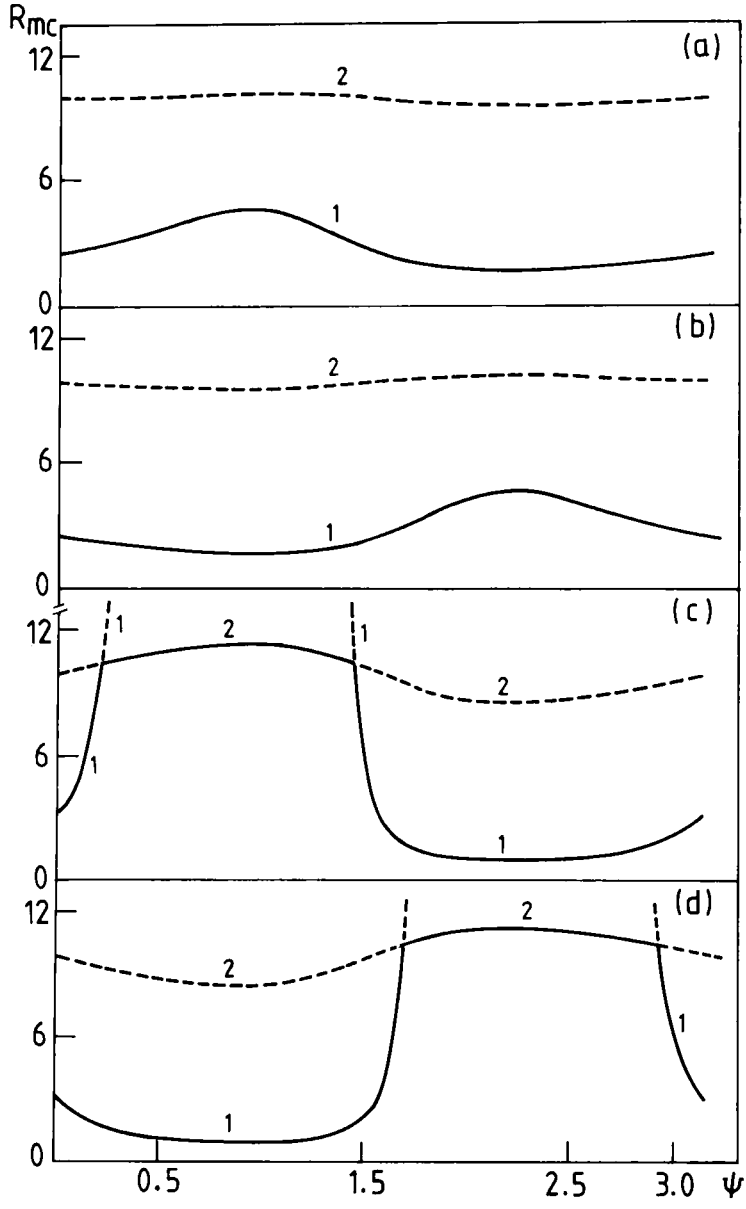

FIGURE 4 *NFAN*.HBAB. Plot of the *HI* field threshold R_{mc} vs field orientation ψ at two shear rates. Curves 1 and 2 represent Modes 1 and 2 respectively. Dashed parts of the curves are not of practical interest.
(a) $|(\Delta T)\cos\varphi| = 0.1°C$; $G = 0.49$; (b) $G = -0.49$.
(c) $|(\Delta T)\cos\varphi| = 0.5°C$; $G = 2.45$; (d) $G = -2.45$.

< 0 are seen to result essentially from a reflection of the curves for $G > 0$ in the R_{mc} axis. For $G > 0$, the thresholds of both modes show an increase when $0 < \psi < \pi/2$ and a decrease over the ψ range $\pi/2 < \psi < \pi$. For $G < 0$, the ψ ranges have to be interchanged.

It is straightforward to appreciate the variation of R_{mc} with ψ at a low shear rate by employing the qualitative arguments used in sec. 3 for a *FAN*. The case of $G > 0$ is considered; for $G < 0$ the arguments are similar. To fix ideas consider again a region of the sample where $3\xi^2 - 1 < 0$. A fluctuation $n_z > 0$ creates the torque $\Gamma_z^{(1)} \sim n_z[A_5 + A_6(3\xi^2 - 1)] < 0$ (Eq. 3) which in turn gives rise to $n_y < 0$. The n_y perturbation creates a torque $\Gamma_y^{(1)} \sim n_y[A_2 + A_3(3\xi^2 - 1)]$. When ψ is close to 0 or $\pi/2$, the magnetic term A_2 is very small but positive. As $\alpha_3 > 0$, $\Gamma_y^{(1)} > 0$ so that the initial n_z perturbation is diminished; the feed-back mechanism is not positive. The only destabilising effect arises from the torques $\Gamma_y^{(2)} \sim -A_1 n_z < 0$ and $\Gamma_z^{(2)} \sim A_4 n_y < 0$. When ψ is close to $\pi/4$, $\sin 2\psi \approx 1$ and A_2 is no longer small. The enhanced, positive contribution from A_2 strengthens the stabilising effect of the positive torque $\Gamma_y^{(1)}$ and this seems to account for the rise in R_{mc} when $\psi \approx \pi/4$. In the ψ range $\pi/2 < \psi < \pi$, both A_2 and A_5 are negative. A_5 can make $\Gamma_z^{(1)}$ more negative. In particular, when $\psi \approx 3\pi/4$, $\sin 2\psi \approx -1$. As $|\alpha_3| \ll 1$, the magnetic term A_2 may outbalance the viscous contribution from A_3 resulting in $\Gamma_y^{(1)} < 0$ which in turn tends to increase the original n_z perturbation. This may qualitatively explain the dip in R_{mc} when $\psi \approx 3\pi/4$.

For shear flow[21] one can calculate the wave vectors at threshold for n_y and n_z. The dominant wave vectors of the two modes crossover at a shear rate close to the crossover point of the field thresholds. This suggests a possible reason for one mode becoming more favourable than the other, the argument being that the larger the wave vector the higher the threshold. Also, the *NP*s of the unfavourable mode are more distorted as compared to the other mode, giving credence to the argument.

In the present case, due to the reasons stated in sec. 2 it is not possible to calculate the wave vectors at threshold for the two modes. One can, at best, appreciate the crossover qualitatively by studying the *NP*s. Figure 5 illustrates the *NP*s at $G = 2.45$ [$(\Delta T) \cos \varphi = 0.5$°C] for different field orientations. At $\psi = 0$, the effective wave vector of distortion (*EWV*) for Mode 2 is higher than that for Mode 1. Consequently, the Mode 2 threshold is higher than the Mode 1 threshold. At $\psi = 0.2$, the Mode 1 profiles are more distorted as compared to those at $\psi = 0$, showing that *EWV* increases for Mode 1; but the reverse is true for Mode 2, with the profiles less distorted

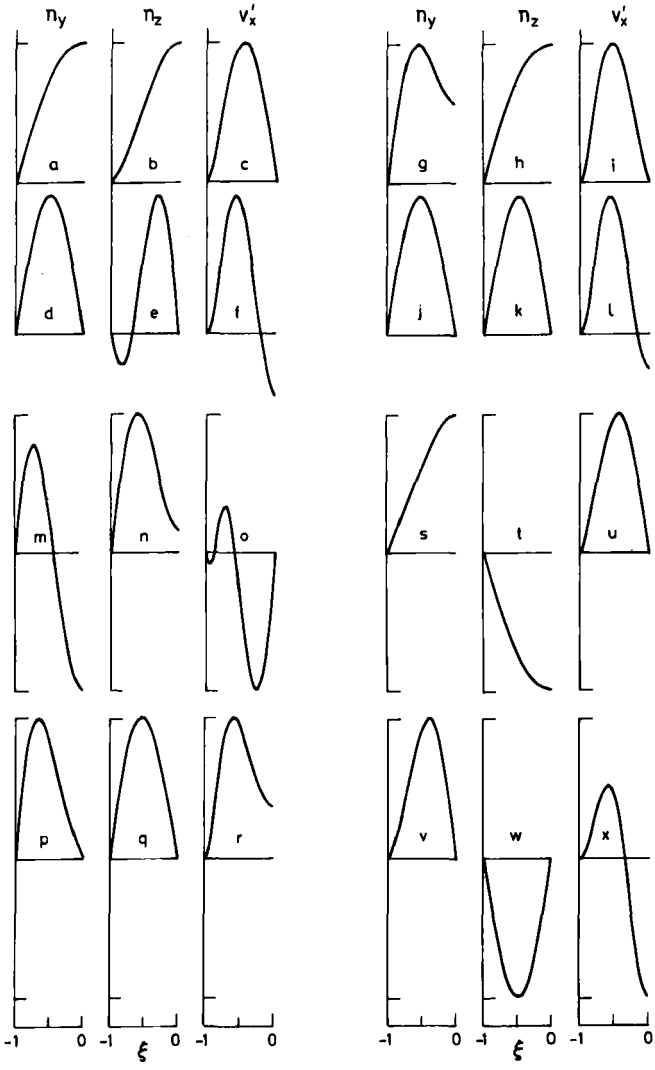

FIGURE 5 *NFAN*.HBAB. Normalised perturbation profiles at field threshold for different field orientations ψ and $G = 2.45$ [$(\Delta T) \cos \varphi = 0.5°C$)]

$\psi = 0$. (a), (b), (c) Mode 1; $H_\perp = 91$, $R_m = 3.2$.
(d), (e), (f) Mode 2; $H_\perp = 159.6$; $R_m = 9.9$.

$\psi = 0.2$. (g), (h), (i) Mode 1; $H_\perp = 155.8$, $R_m = 9.3$.
(j), (k), (l) Mode 2; $H_\perp = 164.4$; $R_m = 10.4$.

$\psi = 0.8$. (m), (n), (o) Mode 1; $H_\perp = 245.1$; $R_m = 18.2$.
(p), (q), (r) Mode 2; $H_\perp = 192.5$; $R_m = 11.2$.

$\psi = 2.2$. (s), (t), (u) Mode 1; $H_\perp = 59.1$; $R_m = 1.0$.
(v), (w), (x) Mode 2; $H_\perp = 174.9$; $R_m = 8.5$.

with respect to those at $\psi = 0$. At $\psi = 0.8$, the Mode 1 profiles are greatly distorted while the Mode 2 profiles are hardly different from those at $\psi = 0.2$. This tentatively points at a possible crossover from Mode 1 to Mode 2 when $\psi \approx 0.8$. The profiles for $\psi = 2.2$ are similar to those for $\psi = 0$, except that the sign of n_z is reversed. The lower *EWV* of the Mode 1 profiles shows that Mode 1 has a lower threshold than Mode 2.

Figure 6 depicts plots of the field threshold (R_{mc}) vs shear rate (G) for a few illustrative field orientations. The diagrams represent the case $G > 0$. At small G, Mode 1 has a lower threshold ($R_{mc} \approx \pi^2/4$) than Mode 2 ($R_{mc} \approx \pi^2$). The R_{mc} values correspond to the Freedericsz threshold and to twice this field, respectively. When $0 < \psi < \pi/2$, both Mode 1 and Mode 2 thresholds increase with G. At sufficiently high G, Mode 2 becomes more favourable than Mode 1. The crossover point ($G = G_0$) is strongly dependent on ψ. Thus, in the above ψ range Mode 2 is generally more favourable than Mode 1 at higher shear rates. At $\psi = 0.8$ or 1.4, in particular, even a second crossover from Mode 2 to Mode 1 seems to be possible at high G (Figure 6a, 6d; $G \approx 24$, $(\Delta T) \cos \varphi \approx 5°C$). However, at high G or ΔT, the Boussinesque approximation is not valid. Hence, this second crossover need not be considered seriously for the present. However, as $G \sim h^3$ (Eqs. 8 and 9) it may be possible to use a thicker sample and bring this crossover point within the permissible ΔT range. It may be recalled that such a second crossover from Mode 2 to Mode 1 is also encountered in shear flow[21] at a high shear rate S_0. This crossover is not of practical interest as the *RI* threshold for shear flow is less than S_0. As the possibility of *RI* has not been studied for free convection, nothing more can be said at present.

As stated earlier, the main destabilising contributions in the case of a *NFAN* arise from the torques $\Gamma_y^{(2)} \sim -A_1 n_z$ and $\Gamma_z^{(2)} \sim A_4 n_y$. When $\psi \approx \pi/4$, A_2 has maximum value and together with A_3, A_2 can contribute a strong stabilising torque $\Gamma_y^{(1)} > 0$. This stabilising contribution from the field term seems to give rise to the initial, rapid increase of R_{mc} with G for Mode 1. However, as G increases further and $H_\perp$ also increases, the destabilising contributions from $\Gamma_y^{(2)}$ and $\Gamma_z^{(2)}$ become stronger and this probably accounts for the later decrease in the Mode 1 threshold.

In the ψ range $\pi/2 < \psi < \pi$, the variation of R_{mc} with G is different. Initially when G is increased, the Mode 1 and Mode 2 thresholds decrease from their respective static values $R_{mc} \approx \pi^2/4$ and π^2. On increasing G further, the thresholds reach their respective minima

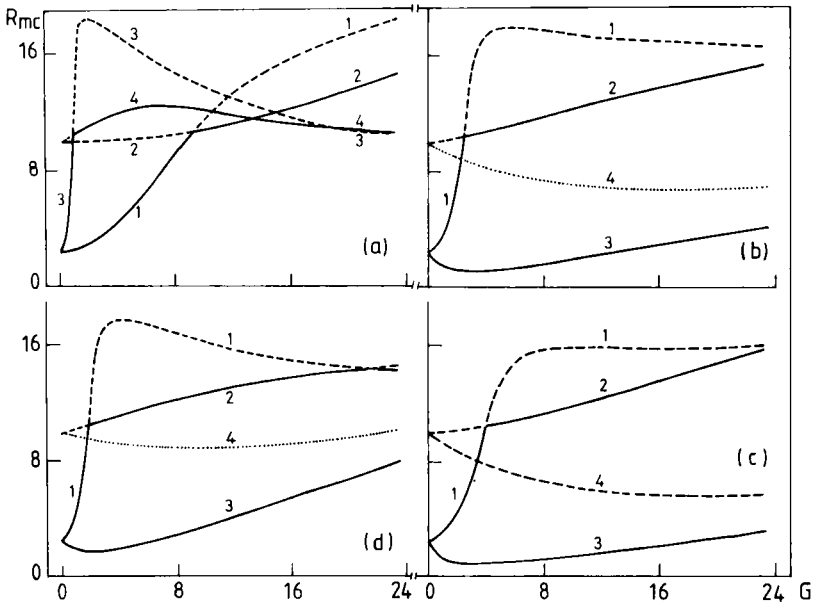

FIGURE 6 *NFAN*.HBAB. Variation of field threshold R_{mc} with shear rate (G) for different field orientations ψ; $G > 0$; Curves 1 and 3 correspond to Mode 1. Curves 2 and 4 represent Mode 2.
(a) $\psi = 0$; (1), (2); $\psi = 0.8$; (3), (4).
(b) $\psi = 0.2$; (1), (2); $\psi = 2.6$; (3), (4).
(c) $\psi = 1.5$; (1), (2); $\psi = 2.2$; (3), (4).
(d) $\psi = 1.4$; (1), (2); $\psi = 2.9$; (3), (4).
Dotted and dashed parts of curves are not of practical interest.

and then start increasing when G takes on still higher values. When $\psi \approx 3\pi/4$ no crossover from Mode 1 to Mode 2 seems to be possible for the shear rates considered. The initial decrease can be seen to be a consequence of A_2 becoming negative. When G is small a negative A_2 can outweigh the stabilising action of A_3, making $\Gamma_y^{(1)} < 0$ and causing a destabilising effect. However, when G increases, A_3 becomes large enough to annul the negative contribution from A_2 and this might explain the increase of R_{mc} with G when G takes larger values.

On the lines of ref. 21, a simple analysis can be made to understand the crossover from Mode 1 to Mode 2 when G increases. The function $3\xi^2 - 1$ is replaced by an average value s and b is ignored. If $\cos q\xi$ and $\sin 2q\xi$ variations are written for Modes 1 and 2 respectively

($q = \pi/2$), Eqs. (2) and (3) reduce to

$$R_{mc}^{(r)} = [(rq)^4 + s^2G^2]/[(rq)^2 + Gsp(\psi)]; \; r = 1, 2;$$

$$p(\psi) = S_\psi C_\psi \zeta/(K_1 C_\psi^2 + K_2 S_\psi^2); \tag{10}$$

$$\zeta = (-\eta_1\alpha_2 - \eta_2\alpha_3)(-K_1K_2/\eta_1\eta_2\alpha_2\alpha_3)^{1/2}$$

For HBAB parameters, $\zeta \approx 4.91 \times 10^{-6}$ dyne. If $s = -\frac{2}{3}$ (= average of $3\xi^2 - 1$ between its zeroes), Eq. (10) is found to describe the variation of R_{mc} with G fairly well at low shear rates. It is found, in particular, that $dR_{mc}^{(1)}/dG > dR_{mc}^{(2)}/dG$ for $0 < \psi < \pi/2$. It is the higher rate of increase of the Mode 1 threshold which is responsible for the crossover from Mode 1 to Mode 2. The reason for this is obviously the smaller elastic energy which is initially associated with Mode 1. To find the crossover point G_0, the Mode 1 and Mode 2 thresholds as given by Eq. (10) are equated for a given ψ. For any value of ψ, there are two solutions

$$G_0(\pm) = q^2[5p \pm (25p^2 + 16)^{1/2}]/2s \tag{11}$$

one of which is positive and the other negative. A substitution shows good accord with Figure 6. For instance, at $\psi = 0, 0.2, 0.8, 1.4, 1.5$, $G_0 = 7.4, 2.3, 0.78, 1.67$ and 3.29, from Eq. (11); the values from Fig. 6 are 9.3, 2.6, 0.9, 1.9, and 3.9. At $\psi = 2.2, 2.6, 2.9$, Eq. (11) yields $G_0 = 72.2, 54.7$ and 27.6 respectively. As these are outside the scope of the present model, they may be ignored.

The *NP*s again afford some insight into the crossover from Mode 1 to Mode 2. Two shear rates and two field orientations have been chosen for the purpose (Figure 7). The shear rates chosen are rather high [$G = 9.75, 19.5$ or $\Delta T = 2°C, 4°C$] from the point of view of the Boussinesque approximation, but serve to illustrate the point. These may also be compared with the corresponding curves from Figure 5 which are drawn for a low shear rate. At $\psi = 0$ (Figure 7a–7l) there is considerable distortion of the Mode 1 profiles when G is increased; but the Mode 2 profiles remain qualitatively similar. One can say that *EWV* of Mode 1 increases faster than that of Mode 2, making a crossover inevitable. For $\psi = 2.2$, there is increased distortion of the Mode 1 profiles, but it is seen that the Mode 2 profiles continue to have a higher *EWV*, as n_y and n_z are odd for Mode 2. Thus a crossover from Mode 1 to Mode 2 is seen to be unlikely.

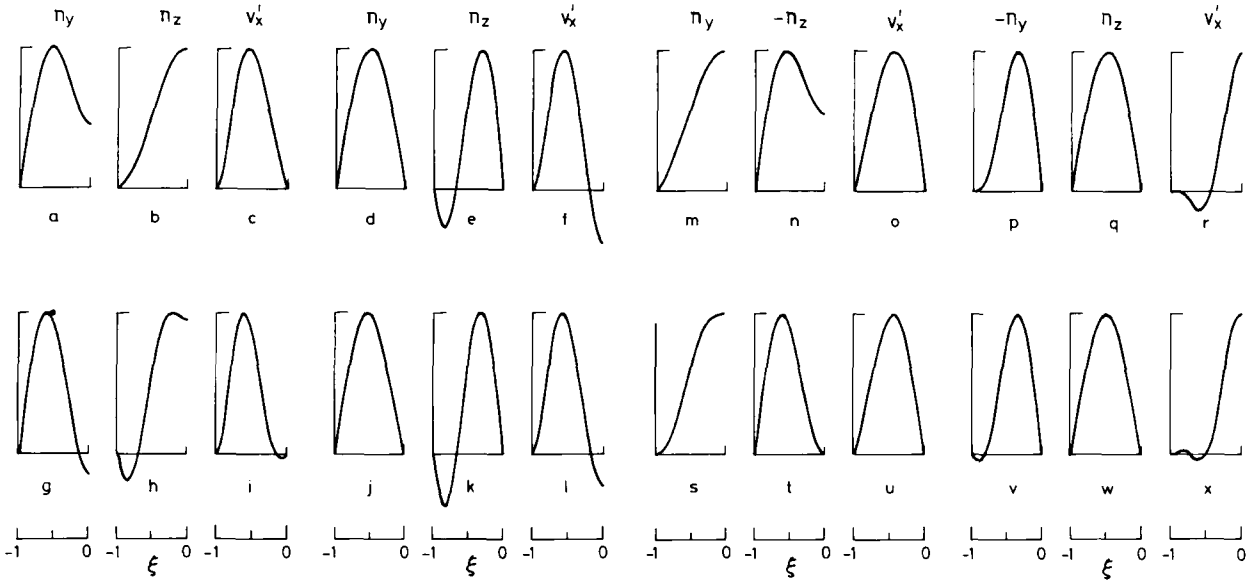

FIGURE 7 *NFAN*.HBAB. Perturbation profiles at field threshold for two different shear rates (G) and field orientations. $X = (\Delta T) \cos \varphi$.
$\psi = 0$; $X = 2.0$; $G = 9.75$; (a), (b), (c) Mode 1; $H_\perp = 169.5$; $R_{mc} = 11.2$;
(d), (e), (f) Mode 2; $H_\perp = 166.4$; $R_{mc} = 10.8$
$\psi = 0$; $X = 4.0$; $G = 19.5$; (g), (h), (i) Mode 1; $H_\perp = 209$; $R_{mc} = 17.0$;
(j), (k), (l) Mode 2; $H_\perp = 184.7$; $R_{mc} = 13.3$.
$\psi = 2.2$; $X = 2.0$; $G = 9.75$;(m), (n), (o) Mode 1; $H_\perp = 72.1$; $R_{mc} = 1.45$;
(p), (q), (r) Mode 2; $H_\perp = 150.2$; $R_{mc} = 6.3$.
$\psi = 2.2$; $X = 4.0$; $G = 19.5$;(s), (t), (u) Mode 1; $H_\perp = 97.9$; $R_{mc} = 2.7$;
(v), (w), (x) Mode 2; $H_\perp = 142.7$; $R_{mc} = 5.7$.

Before going over to the concluding section, brief mention may be made about the predictions of the linearised perturbation model for a *NFAN* with $\chi_a < 0$. As mentioned in sec. 3, viscosity data on nematics with $\chi_a < 0$ do not seem to be available. Hence, in the present work, a model calculation has been performed by adopting the HBAB parameters with the sign of χ_a reversed. As the field $H_\perp$ always stabilises the initial director orientation, the only field of interest is $H_\parallel$ which has a destabilising effect. A preliminary calculation shows that a crossover from Mode 1 to Mode 2 is possible at sufficiently elevated shear rates G.

5. LIMITATIONS OF THE MODEL AND OTHER POSSIBILITIES

In conclusion, the limitations of the mathematical model used in the present work must be clearly stated. Firstly, firm anchoring has been assumed for the director orientation. Secondly, the perturbations have been assumed to be linear. A more thorough investigation is called for, especially in the light of the anomalous variation of the shear threshold for a *FAN* at certain field orientations. The question that requires answer is, whether a nonlinear perturbation calculation will show an ultimate decrease of G_c to zero when the field approaches the Freedericsz transition, despite the initial increase of G_c at low fields. Experiments will naturally point the way in this matter. Thirdly, the sample has been assumed to be infinite along x and y. The effect of finite sample width on the occurrence of Mode 2 (which is associated with net secondary flow) may be profound in a real situation; the occurrence of domains along the primary flow, as happens for plane Poiseuille flow,[11] cannot be ruled out. Fourthly, the occurrence of *RI* can put a limit on the realm of existence of *HI*. For a *NFAN*, the results of sec. 4 conform to the thought experiment in which one starts with the director orientation $\mathbf{n}_0$ at a given shear rate or G and increases $H_\perp$ from zero till the *HI* threshold is realised. If at that G the *RI* can set in, calculations on *HI* beyond this G value will not be realistic. The *RI* calculations here will be more complicated than those for shear flow as the temperature fluctuations have also to be included. These calculations are postponed for a future communication. Lastly, the present model which is based on the Boussinesque approximation cannot be valid for large ΔT or G. However, flow situations at large G may be effectively simulated at lower ΔT values in thicker samples (Eq. 8) unless other complications set in, such as

boundary layer flow. The use of thicker samples may also facilitate observation of crossover between modes which occurs at high G for certain field orientations (Figure 6).

The flow behaviour of nematics with $\chi_a < 0$ is found to be markedly different from that of the other nematics. Detailed theoretical studies will be justified if such materials are studied more thoroughly in experiments and also if estimates of their viscous properties are made. Till then, a study like the one made here or in ref. 21 will remain rather speculative.

The oblique field configuration studied by Deuling *et al.*[20] has been extended to two other flow situations. In the case of *HI* in the flow aligning configuration studied by Leslie[29] the crossover between modes is found to be strongly dependent on the field orientation relative to the shear plane, the field remaining in a plane normal to the flow aligned nematic director. Details will be published shortly.[31] The other case is *HI* in plane Poiseuille flow. As mentioned in ref. 21, an oblique field destroys the modal structure, seeming to mix up the splay and twist modes. A preliminary study shows that the threshold is strongly dependent on the field orientation. Results will be communicated in the future.[32]

References

1. P. G. De Gennes, *The Physics of Liquid Crystals* (Clarendon Press, Oxford, 1974).
2. S. Chandrasekhar, *Liquid Crystals* (Cambridge University Press, Cambridge, 1977).
3. J. L. Ericksen, *Advances in Liquid Crystals* (Volume 3, Ed. G. H. Brown, Academic Press, New York, 1979).
4. F. M. Leslie, *Advances in Liquid Crystals* (Volume 4, Ed. G. H. Brown, Academic Press, New York, 1979).
5. P. Pieranski and E. Guyon, *Solid State Commun.*, **13**, 435 (1973).
6. P. Pieranski and E. Guyon, *Phys. Rev.*, **A9**. 404 (1974).
7. E. Guyon and P. Pieranski, *Physica*, **73**, 184 (1974).
8. E. Guyon and P. Pieranski, *J. Physique*, **36(C1)**, 203 (1975).
9. P. Manneville and E. Dubois-Violette, *J. Physique*, **37**, 285 (1976).
10. F. M. Leslie, *J. Phys.*, **D9**, 925 (1976).
11. I. Janossy, P. Pieranski and E. Guyon, *J. Physique*, **37**, 1105 (1976).
12. P. Manneville and E. Dubois-Violette, *J. Physique*, **37**, 1115 (1976).
13. E. Dubois-Violette, G. Durand, E. Guyon, P. Manneville and P. Pieranski, *Solid State Physics Supplement 14*, **147** (Academic Press, 1978).
14. D. Horn, E. Guyon and P. Pieranski, *Rev. Physique Appl.*, **11**, 139 (1976).
15. P. Pieranski and E. Guyon, *Phys. Rev. Lett.*, **32**, 924 (1974).
16. P. Pieranski and E. Guyon, *Commun. Phys.*, **1**, 45 (1976).
17. E. Guyon, P. Pieranski and S. A. Pikin, *J. Physique*, **37**, (C1) 3 (1976).
18. U. D. Kini, *Pramana*, **15**, 231 (1980).
19. U. D. Kini, *Mol. Cryst. Liquid Cryst.*, **99**, 223 (1983).
20. H. Deuling, M. Gabay, E. Guyon and P. Pieranski, *J. Physique*, **36**, 689 (1975).

21. U. D. Kini, *Mol. Cryst. Liquid Cryst.*, **116**, 1 (1984).
22. B. A. Finlayson, *The Method of Weighted Residuals and Variational Principles* (Academic Press, 1972).
23. H. C. Tseng, D. L. Silver and B. A. Finlayson, *Phys. Fluids*, **15**, 1213 (1972).
24. L. D. Landau and E. M. Lifshitz, *Fluid Mechanics* (Pergamon Press, 1966).
25. L. Pohl, R. Eidenschink, J. Krause and G. Weber, *Phys. Lett.*, **A65**, 169 (1978).
26. H. Schad and M. A. Osman, *J. Chem. Phys.*, **75**, 880 (1981).
27. K. P. Sinha, R. Subburam and C. L. Khetrapal, *Chem. Phys. Lett.*, **96**, 472 (1983).
28. L. J. Yu and A. Saupe, *Phys. Rev. Lett.*, **45**, 1000 (1980).
29. F. M. Leslie, *Mol. Cryst. Liquid Cryst.*, **37**, 335 (1976).
30. U. D. Kini, *Liquid Crystals* (S. Chandrasekhar, editor, Heyden, 1980) 255.
31. U. D. Kini, work in progress.
32. U. D. Kini, *Mol. Cryst. Liquid Cryst.* (submitted).